JMEPEG (2017) 26:4748–4759
DOI: 10.1007/s11665-017-2918-x


1059-9495/$19.00

# Correlation Between Microstructure and Corrosion Resistance of Magnesium Alloys Prepared by High Strain Rate Rolling

*Jihua Chen, Guanqing Chen, Hongge Yan, Bin Su, Xiaole Gong, and Bo Zhou*

*(Submitted February 26, 2017; in revised form June 20, 2017; published online September 8, 2017)*

**Microstructure and corrosion resistance in Hank's solution of four magnesium alloys (pure Mg, ZK60, Mg-4Zn and Mg-4Zn-0.3Ca) prepared by high strain rate rolling (HSRR) and conventional rolling (CR) are comparatively investigated. The HSRR alloy exhibits better bio-corrosion resistance than the CR alloy. The HSRR ZK60 alloy has finer grains, higher dynamic recrystallization (DRX) extent, lower twin fraction, coarser residual second-phase particles, finer and denser nanometer $\beta_1$ precipitates, lower residual compressive stress and stronger basal texture than the CR alloy. The average corrosion rate of the HSRR ZK60 sheet after 90-day immersion in Hank's solution is 0.17 mg $cm^{-2}$ $d^{-1}$, about 19% lower than that of the CR sheet. Its corrosion current density is 30.9 μA/$cm^2$, about 45% lower than that of the CR sheet. Bio-corrosion resistance enhancement by HSRR can be mainly ascribe to the reduced grain size, the relatively adequate DRX, non-twinning, the coarser residual second-phase particles, the finer and denser nanometer precipitates and the slightly stronger (0001) texture.**

**Keywords** corrosion resistance, high strain rate rolling microstructure, nanometer precipitate, wrought magnesium alloy

## 1. Introduction

Magnesium (Mg) and its alloys have been investigated since as early as 1878 for their potential use as a biomaterial (Ref 1). However, pure Mg corrodes too rapidly in vivo, losing mechanical integrity before the tissue has sufficiently healed (Ref 2). Several measures such as alloying, change in the processing histories and surface modification have been adopted to improve the biodegradation property.

The processing histories have significant influences on the bio-corrosion resistance of magnesium alloys. According to Wang H et al., the biodegradation rate of AZ31 in Hank's solution can be significantly reduced by mechanical processing and the desirable retardation of the excessively rapid degradation can be provided by hot rolling, but additional ECAP processing does not lead to further deceleration of corrosion (Ref 3). Shervin Eslami Harandi et al. have investigated the effect of forging process parameters on a binary Mg-1Ca alloy as a biodegradable bone implant material and have found that more hydroxyapatite product is generated in the alloy exposed to the SBF by elevating forging temperature during corrosion process while increasing forging speed brings about a decrease in the product (Ref 4). According to H.Y. Choi et al., the combination of solid solution heat treatments and severe plastic deformation by high-ratio differential speed rolling (HRDSR) results in the formation of an ultrafine-grained microstructure with high thermal stability, high corrosion resistance, high strength and high ductility and excellent superplasticity in a ZK60 alloy, which allows the fabrication of biodegradable magnesium devices with complicated designs that have a high mechanical integrity throughout the service life in the human body (Ref 5). P. Minárik et al. have studied corrosion properties of AE21 and AE42 magnesium alloys in the extruded state and after subsequent eight passes of equal channel angular pressing (ECAP) via route Bc and have found that the lower corrosion resistance in AE21 alloy after the ECAP is caused by the grain refinement and the effect of grain size is suppressed by better distribution of Al containing dispersed particles resulting in significantly better corrosion resistance of the fine-grained microstructure in AE42 alloy (Ref 6). Thermo-mechanical processing can influence the grain size and the distribution of alloying elements through the material and therefore manage the overall corrosion resistance of the alloy (Ref 6, 7). Gao J H et al. have found that high-pressure torsion can improve the bio-corrosion resistance of the Mg-Zn-Ca alloy (Ref 8). However, it is also reported that grain refinement through severe plastic deformation (SPD) (Ref 9) is found to be detrimental to corrosion resistance improvement of Mg alloys.

It is well known that the processing histories have significant influences on the mechanical properties of magnesium alloys. It is reported that of AZ31 magnesium alloy sheets with good mechanical properties can be processed by repeated cold rolling and annealing using a small pass reduction and the grain microstructure of AZ31 alloy sheet can be successfully refined to 7.4 μm after 87% total repeated cold rolling reduction and annealing, which exhibits good deep drawability (Ref 10, 11). In recent years, our research group has devoted much effort to

**Jihua Chen, Guanqing Chen, Hongge**, and **Yan Bin Su**, School of Materials Science and Engineering, Hunan University, Changsha 410082, China; and Hunan Provincial Key Laboratory of Spray Deposition Technology and Application, Hunan University, Changsha 410082, China; **Xiaole Gong** and **Bo Zhou**, School of Materials Science and Engineering, Hunan University, Changsha 410082, China; Contact e-mails: jihuachen@hnu.edu.cn. jihuachen2005@163.com.

prepare high-performance wrought magnesium alloy sheets by high strain rate rolling (HSRR) and fine-grained sheets with the average grain size less than 5 μm and good combination of strength and plasticity are available (Ref 12, 13). HSRR is a novel rolling method that inhibits cracking through the preferred initiation of twinning and the subsequent recrystallization (Ref 12) and is beneficial for the enhanced plasticity in magnesium alloys (Ref 13). The HSRRed Mg-4Zn alloy sheet exhibits different bio-corrosion behavior from the as-cast, and its in vitro strength loss is about 19% after 7-day immersion in 0.9 wt.%NaCl solution (the as-cast, 62%) (Ref 14). It also shows the lowest average corrosion rate of 0.25 mg/cm$^2$ d, about 1/5 of the as-cast alloy after soaking in Hank's solution for 15 days and the highest corrosion residual tensile strength (215 MPa), far above the as-cast and the solutionized alloys (Ref 15). Our preliminary data show that the alloy prepared by high strain rate rolling (HSRR) exhibits better bio-corrosion resistance than the alloy prepared by conventional rolling (CR) (Ref 16). However, the mechanism for bio-corrosion resistance improvement of magnesium alloys prepared by HSRR remains unclear. Therefore, the main goal of the study is to explore the mechanism for bio-corrosion resistance improvement of magnesium alloys prepared by HSRR in view of microstructure characteristics.

## 2. Experimental Details

### 2.1 Materials and Characterization

The Mg-4Zn and Mg-4Zn-0.3Ca alloys (in wt.%) were prepared by gravity casting in an electric resistance furnace with a mild steel crucible protected by the RJ-2 flux (37.1% KCl—43.2% $MgCl_2$—6.8% $BaCl_2$—4.8% $CaF_2$—6.6% (NaCl + $CaCl_2$)—1.3% water-insoluble—0.4% moisture, in wt.%). Commercially pure Mg, pure Zn stuffs (99.9%) and Mg-20Ca alloy were added to prepare the alloy. The melt was purged at 720 °C for 10 min and held for 15 min at 760 °C so that homogenization of alloying elements and settlement of inclusions can be realized. Then, molten alloy was cast into a water-cooling steel mold (100 mm × 150 mm × 20 mm) at a casting temperature of 720 °C. The mold was made of the 0.45%C carbon steel. Pure Mg (99.99%) and semi-continuous castings of ZK60 were also adopted.

Block specimens were cut from the as-cast plates. The Mg-4Zn alloy was homogenized at 300 °C for 2 h and 330 °C for 30 h before rolling. The Mg-4Zn-0.3Ca alloy was homogenized at 300 °C for 2 h, 330 °C for 30 h and 430 °C for 2 h before rolling. The ZK60 alloy was homogenized at 300 °C for 2 h, 330 °C for 28 h and 400 °C for 4 h before rolling. HSRR and CR were adopted in the experiments. These blocks with the thickness of 10 mm were preheated to a setting temperature for 6 min before rolling, and the rolls are not heated. The linear velocity of the rollers was 430 mm/s. Some blocks were rolled by a single pass to the final thickness ($h$ = 2 mm) with the thickness reduction λ about 80%, and the average strain rate was 9.32 s$^{-1}$, which was named as HSRR. The detailed information about HSRR could be found in the literature (Ref 12, 13). Some blocks were rolled by three passes to the final thickness of about 2 mm (10 mm-6 mm-4 mm-2 mm) and with the total reduction about 80%, which was named as CR. The average strain rate was 1.6 s$^{-1}$.

The microstructural observation of the as-rolled alloys was conducted on a MM-6 metallographic microscope and the FEI QUANTA 200 scanning electron microscopy (SEM) after etching with a solution of 0.6-1.2 g picric acid, 2 ml acetic acid, 3 ml water and 20 ml ethanol. The average grain size was calculated according to the GB-T-6394-2002 standard. The volume fraction of DRX (dynamic recrystallization) grains was calculated using the Image-Pro Plus 6.0 software. The phase constitutions of the as-rolled ZK60 alloys were analyzed by a D5000 x-ray diffraction (XRD) instrument with Cu Kα and a scanning rate of 0.01 °/s. The microstructural characteristics of the as-rolled sheets were further examined by a Titan G2 60-300 transmission electron microscopy (TEM). The residual stress and the texture analysis were conducted on a D8 tool XRD instrument with Cu Kα, the accelerated voltage of 40 kV and the electric current of 40 mA. The sample for residual stress measurement is with the size of 10 mm × 10 mm × 2 mm, while that for texture analysis is with the size of 8 mm × 6 mm × 2 mm and is chemically polished before testing.

### 2.2 Static Immersion Tests

For static immersion testing, the samples with the size of 20 mm × 15 mm × 2 mm were ground successively with SiC paper up to 1500 grit and cleaned in acetone. The surface area of each specimen was about 7.4 cm$^2$. The Hank's solution (0.14 g/L $CaCl_2$, 0.4 g/L KCl, 8.0 g/L NaCl, 0.1 g/L $MgSO_4$, 0.06 g/L $KH_2PO_4$, 0.05 g/L $Na_2HPO_4$ and 1.0 g/L D-Glucose) (Ref 3) was used in the immersion tests. The polished and pre-weighed samples were exposed to the solution (150 ml, Hank's solution) at 37 ± 0.5 °C for various intervals of time, i.e., 12 h, 3, 7, 15, 30, 60 and 90 days. The solution volume/surface area ratio was fixed at 20.3 ml/cm$^2$. Ultrasonic cleaning of the sample at the end of the experiment was done by dipping it in a solution of the 200 g/L $CrO_3$ + 10 g/L $AgNO_3$ solution for 5 min and then in ethanol for 10 min to remove the corrosion product. Finally, the immersed sample was dried in the warm flowing air. The as-corroded surface morphologies were recorded. The weight loss $\Delta W$ was measured after each experiment.

The average corrosion rate was adopted to evaluate the bio-corrosion degradation behavior. The former was the relative value of the weight loss to the original weight of the immersion sample, while the latter was calculated by the following equation.

$$R = \Delta W/(At)$$

where $R$ was the corrosion rate, mg/cm$^2$/d; $\Delta W$ was the weight loss, mg; $A$ was the original surface area exposed to the test solution, cm$^2$; and $t$ was the exposure time, day. The corrosion rate was averaged over three specimens.

### 2.3 Electrochemical Measurement

Electrochemical polarization experiments were carried out using a CHI 600B potentiostat in Hank's solution at 37 ± 0.5 °C. For all the experiments, a three-electrode cell was used, with a saturated calomel electrode (SCE) as a reference electrode and a platinum counter electrode. The work electrode consisted of a cylinder rod, which was prepared by connecting a copper wire to one side of the sample and was embedded in the epoxy resin to provide insulation. The

opposite surface of the sample was exposed to the solution. The exposed area was 10 mm × 10 mm. The samples were given a metallographic polishing with SiC paper up to 1500 grit prior to each experiment, followed by washing with the distilled water and acetone. The open circuit versus time curve was recorded for 10 min at first, and then the polarization curve of the sample started from −250 mV relative to the corrosion potential and moved toward more noble values at a potential scanning rate of 1 mV/s. In each case, duplicate experiments were conducted. All the experiments were controlled by the computer, which was also used for the acquisition, the storage and the plotting of data. The corrosion potential ($E_{corr}$) and corrosion current density ($i_{corr}$) were averaged over three specimens.

## 3. Results

### 3.1 Microstructure Characteristics

All the alloys are homogenized before rolling, and the amount of the residual intermetallic phases in each alloy is relatively low. Optical images of the as-rolled magnesium alloys prepared by HSRR and CR are shown in Fig. 1. The average grain sizes and the DRX volume fractions of the as-rolled sheets are listed in Table 1. As shown in Fig. 1(a) and (b), the HSRR pure Mg is featured with full DRX and with the average grain size of 7.7 μm, while that of CR is characteristic of the DRX volume fraction of 40% and the average grain size of 37.7 μm. As shown in Fig. 1(c) and (d), the HSRR Mg-Zn alloy is featured with full DRX and with the average grain size of 3.7 μm, while that of CR is characteristic of the DRX volume fraction of 75% and the average grain size of 7 μm. As shown in Fig. 1(e) and (f), the HSRR Mg-Zn-0.3Ca alloy is featured with almost full DRX and with the average grain size of 3 μm, while that of CR is characteristic of the DRX volume fraction of 76% and the average grain size of 7.5 μm.

As shown in Fig. 1(g) and (h), the HSRR ZK60 alloy is featured with the DRX volume fraction of 90% and with the average grain size of 2.6 μm, while that of CR is characteristic of the DRX volume fraction of 60% and the average grain size of 8 μm. Obviously, the rolling mode has a great influence on the as-rolled microstructures. The HSRR sheet exhibits the higher DRX extent, the finer grain size and fewer twins than the corresponding CR sheet. As reported in the literature (Ref 12), an ultrafine-grained microstructure with a low dislocation density can be obtained by a large amount of DRX, especially DRX on twins, and microstructural homogeneity can be improved by the high twin density and the consequent large fraction of DRXed grains as the rolling strain rate rises.

The XRD patterns of the as-rolled ZK60 sheets prepared by HSRR and CR are shown in Fig. 2. Both alloys are composed of two phases, i.e., α-Mg and $Mg_7Zn_3$. Moreover, the peaks at approximately 45° and 65° are likely to be the $\beta_1$ phase. The SEM images of the as-rolled ZK60 sheets prepared by HSRR and CR are shown in Fig. 3. As marked by the black circles, the intermetallics in the HSRR ZK60 sheet are in granular and are distributed along the primary grain boundaries, while those in the CR sheet are broken and are elongated along the rolling direction. These intermetallics are the undissolved phase during homogenization. In compared with the CR sheet, the broken residual second-phase particles in the HSRR are relatively coarse. The EDS analysis shows that the particles in the HSRR sheet are composed of 55.44 at.%Mg, 33.35 at.%Zn and 10.99 at.%Zr, while those in the CR sheet are composed of 86.21 at.%Mg, 11.34 at.%Zn and 2.28 at.%Zr.

The TEM images of the as-rolled ZK60 sheets prepared by HSRR and CR are shown in Fig. 4. As seen from Fig. 4(a) and (b), some fine DRX grains with the grain size about 1 μm are detected, while some traces of twins are also existent in the HSRR sheet. As seen from Fig. 4(c) and (d), the trigeminal grain boundaries are clean in the HSRR sheet and no coarse precipitates are detected at grain boundaries. However, high-density nanometer precipitates with the size of 10 nm are distributed in the grain interiors. As seen from Fig. 4(e) and (f), some dislocation tangling is detected and many twins are existent in the CR sheet. As seen from Fig. 4(g) and (h), the trigeminal grain boundaries are relatively clean in the CR sheet and almost no coarse precipitates are detected at grain boundaries. Likewise, high-density nanometer precipitates with the size of 20 nm are distributed in the grain interiors. The STEM images and elemental mappings of the as-rolled ZK60 sheets are shown in Fig. 5. Obviously, the nanometer precipitates in the grain interiors of the HSRR sheet are much finer and denser than those in the CR sheet. Moreover, these precipitates are rich in Zn. On the basis of the literatures on aging precipitates in the Mg-Zn alloy system, these nanometer precipitates are inferred to be the $\beta_1$ phase.

Residual stress distribution characteristics of the as-rolled ZK60 sheets prepared by HSRR and CR are shown in Fig. 6. The detailed residual stress data are listed in Table 2. According to the European Standard, the HSRR ZK60 sheet has the residual normal stress of $-77.7 \pm 16.4$ MPa and the residual shear stress of $18.6 \pm 8.2$ MPa, while the CR sheet has the residual normal stress of $-89.2 \pm 11.8$ MPa and the residual shear stress of $13.2 \pm 5.9$ MPa. According to the Chinese Standard, the HSRR ZK60 sheet has the residual stress of $-44.6 \pm 13.2$ MPa, while the CR sheet has the residual stress of $-65.7 \pm 9.4$ MPa. Both sheets are featured with the residual normal compressive stress state. Moreover, the HSRR ZK60 sheet exhibits the higher residual shear stress but the lower residual normal stress than the CR sheet.

As stated above, the HSRR sheet exhibits the higher DRX extent, the finer DRX grain size and fewer twins than the corresponding CR sheet. As seen from Fig. 4, some dislocation tangling and many twins are existent in the CR sheet, indicating that the high storage energy is involved. Thus, the CR ZK60 sheet exhibits the higher residual compressive stress than the HSRR sheet.

The (0001) pole figures at surface layers of the as-rolled ZK60 sheets prepared by HSRR and CR are shown in Fig. 7. The basal texture with the basal planes oriented toward the rolling direction is detected, which is a typical texture of the as-rolled and the as-extruded alloys. The central pole density of the HSRR ZK60 sheet is 5.23, while that of the CR sheet is 4.35. The higher basal texture peak intensity and the more scattered pole density center indicate that the ZK60 sheet prepared by HSRR has a slightly stronger basal texture than the sheet prepared by CR. However, it is reported that the AZ31 sheet prepared by HSRR exhibits a weaker basal texture than that prepared by CR (Ref 17). The most likely reason is that the rotation of the DRX grains and sub-grains can be effectively hindered by the pinning of nanometer precipitates in the HSRR ZK60 sheet, but the effect of pinning will be weakened due to

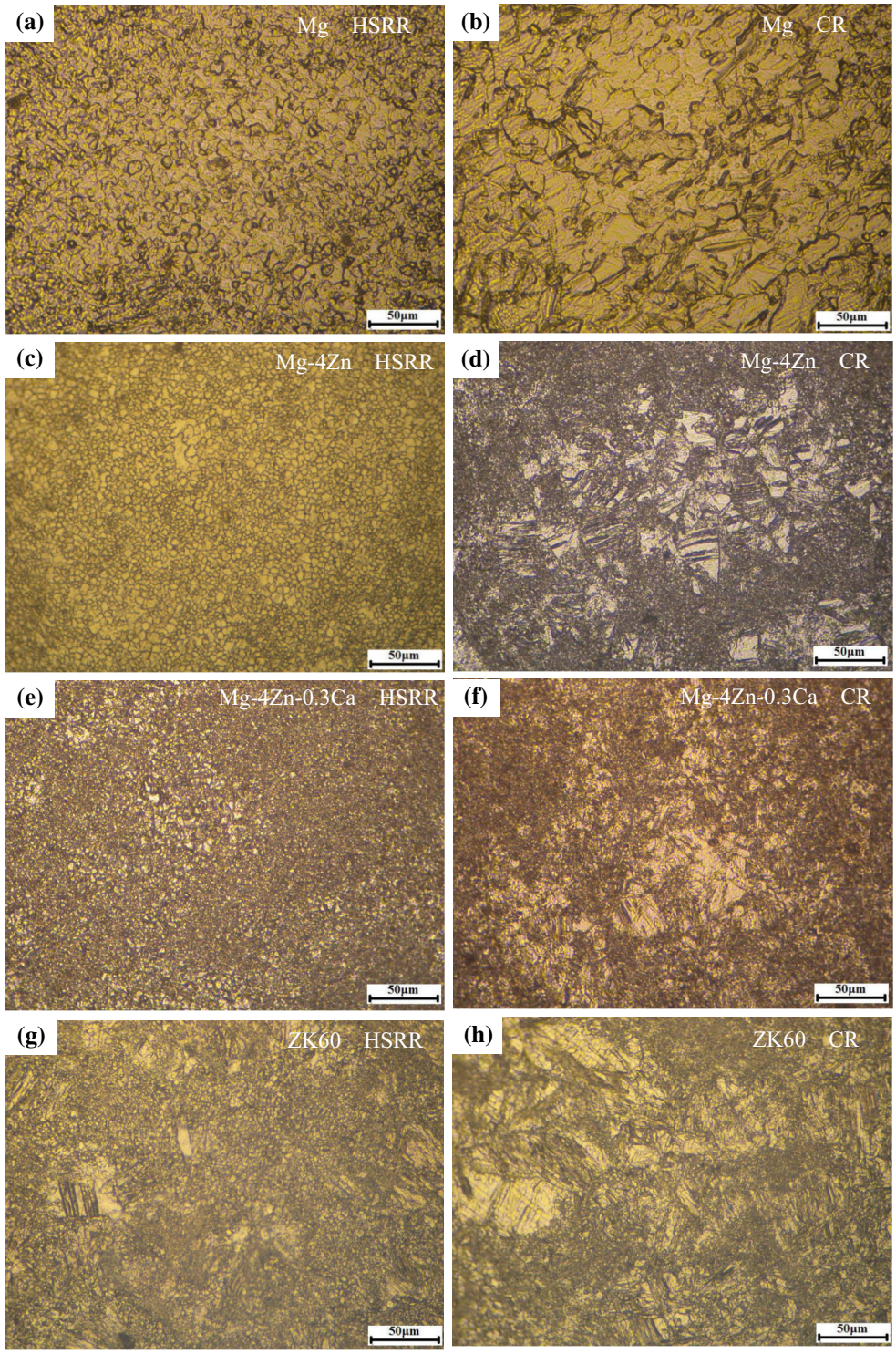


**Fig. 1** Optical images of the as-rolled magnesium alloys prepared by HSRR and CR

**Table 1 Average grain sizes and DRX volume fractions of the as-rolled sheets**

| | Pure Mg | | Mg-4Zn | | Mg-4Zn-0.3Ca | | ZK60 | |
|---|---|---|---|---|---|---|---|---|
| **Alloys** | **HSRR** | **CR** | **HSRR** | **CR** | **HSRR** | **CR** | **HSRR** | **CR** |
| Average grain size, μm | 7.7 | 33.7 | 3.7 | 7 | 3 | 7.5 | 2.6 | 8 |
| Volume fraction of DRX, % | 100 | 40 | 100 | 75 | 97 | 76 | 90 | 60 |

the coarsening of the precipitates in the CR sheet. The detailed reason remains unclear.

### 3.2 Constant Immersion and Electrochemical Studies

**3.2.1 Weight Loss and The Average Corrosion Rate.** Relationships between the average corrosion rate and the soaking time of the as-rolled magnesium alloys prepared by HSRR and CR in Hank's solution at 37 °C are shown in Fig. 8.

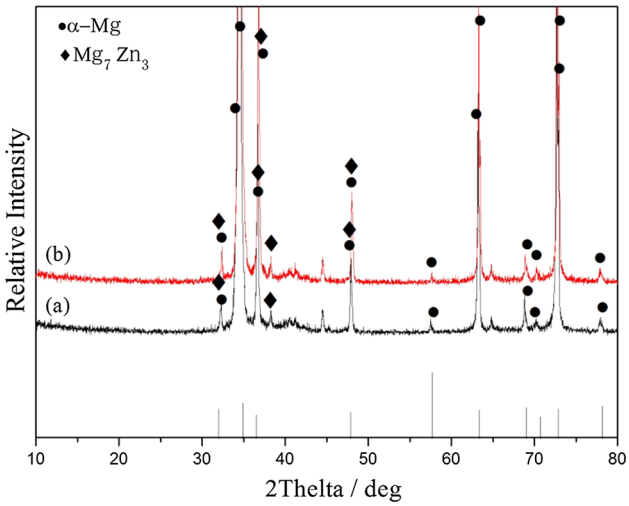


**Fig. 2** XRD patterns of the as-rolled ZK60 sheets prepared by HSRR (a) and CR (b)

Obviously, all the as-rolled magnesium alloys have the same bio-corrosion degradation behavior. With a prolonged immersion time, the corrosion rates of the as-rolled alloys have a decreasing tendency up to 30 days and then keep at the relatively constant levels. The observed decrease in the degradation rate with the immersion time is consistent with the bio-corrosion behavior of the AZ31 alloys prepared by squeeze casting, hot rolling and equal channel angular pressing (Ref 3). However, the alloy prepared by CR exhibits the higher corrosion rate than the corresponding alloy prepared by HSRR after different time immersion. As far as pure Mg is concerned, the average corrosion rates of both sheets prepared by CR and HSRR are relatively low among all the as-studied alloys. The as-rolled pure Mg sheet prepared by HSRR exhibits the lower corrosion rate than that prepared by CR with the immersion time of 7 days or shorter, while it exhibits the higher corrosion rate with the immersion time of 15 days or longer.

The average corrosion rate of the Mg-4Zn alloy prepared by HSRR after 7 days immersion is 0.37 mg $cm^{-2}$ $d^{-1}$, about 33% lower than the CR sheet. Its average corrosion rate after 90 days immersion is 0.16 mg $cm^{-2}$ $d^{-1}$, slightly higher than that prepared by CR. The average corrosion rate of the Mg-4Zn-0.3Ca alloy prepared by HSRR after 7 days immersion is 0.54 mg $cm^{-2}$ $d^{-1}$, slightly lower than the CR sheet. Its average corrosion rate after 90 days immersion is 0.14 mg $cm^{-2}$ $d^{-1}$, about 33% lower than the CR sheet. The average corrosion rate of the ZK60 alloy prepared by HSRR after 3 days immersion is 0.59 mg $cm^{-2}$ $d^{-1}$, about 29% lower than the CR sheet. The average corrosion rate of the ZK60 alloy prepared by HSRR after 7 days immersion is 0.36 mg $cm^{-2}$ $d^{-1}$, about 14% lower than the CR sheet. Its

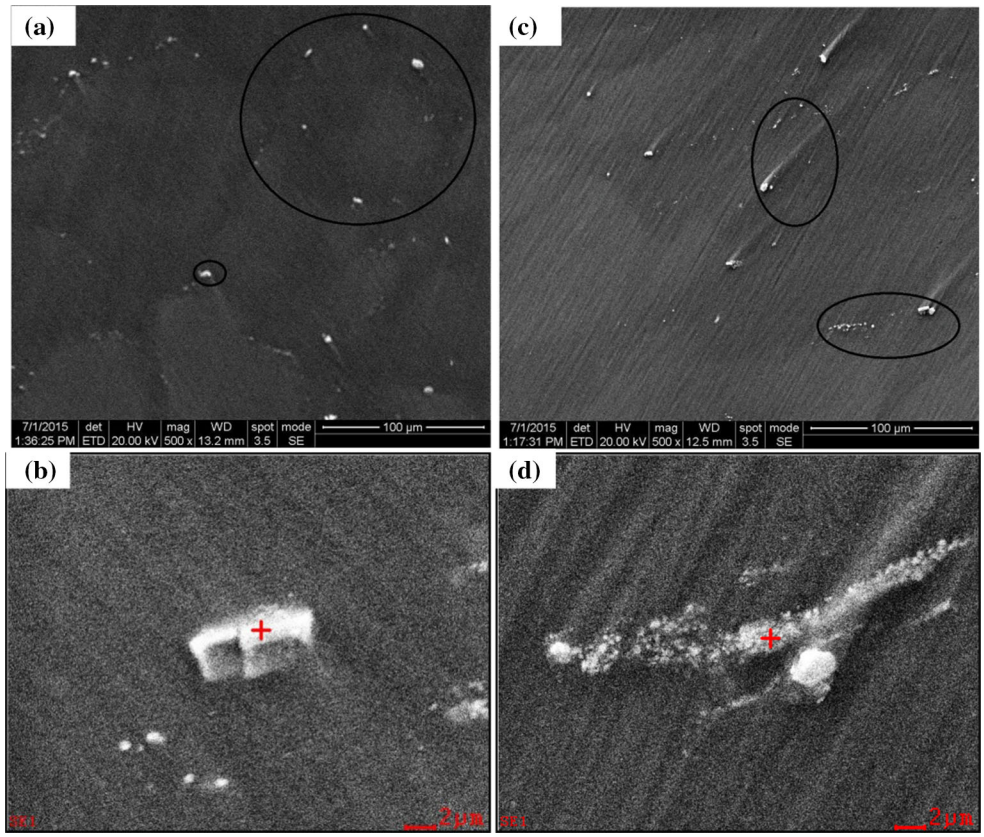


**Fig. 3** SEM images of the as-rolled ZK60 sheets prepared by HSRR (a) (b) and CR (c) (d)

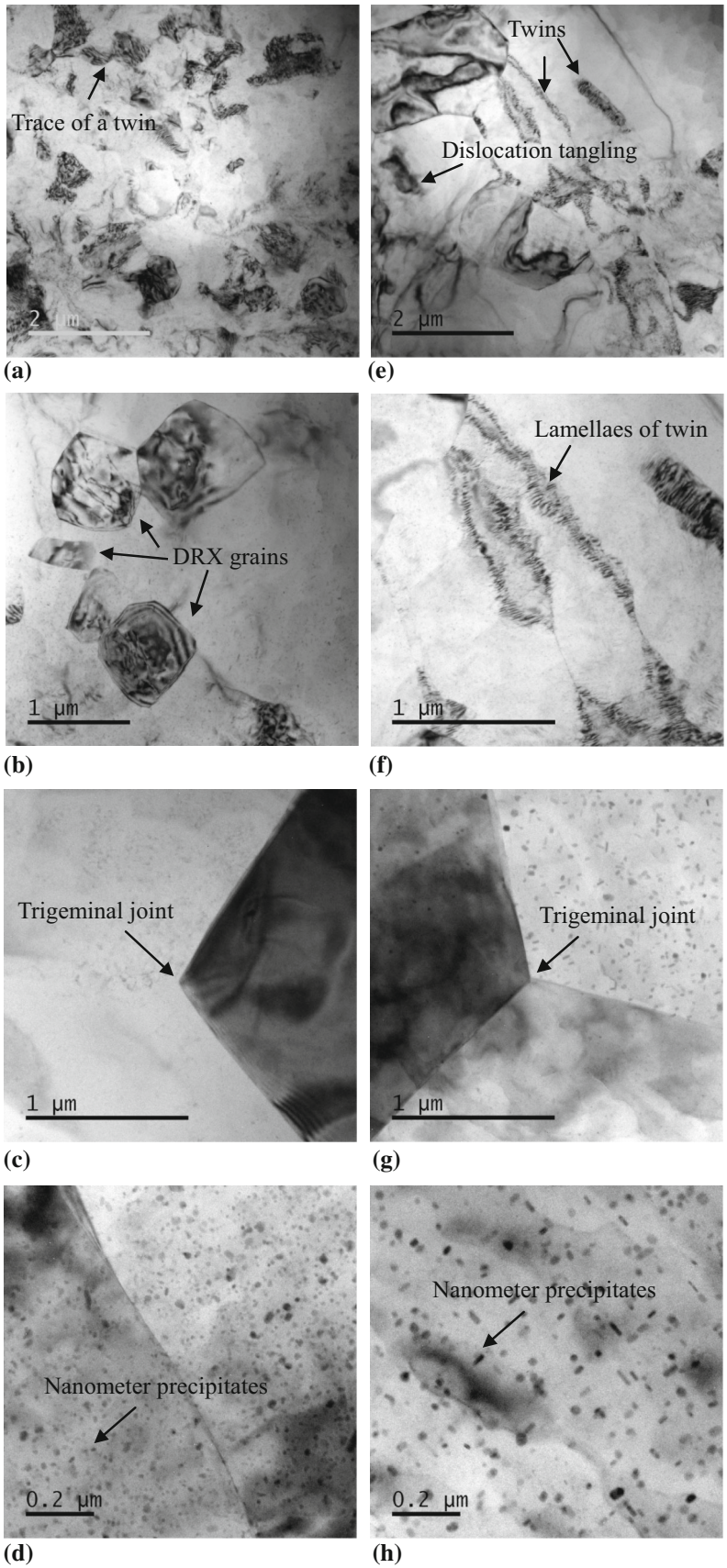


**Fig. 4** TEM images of the as-rolled ZK60 sheets prepared by HSRR (a-d) and CR (e-h)

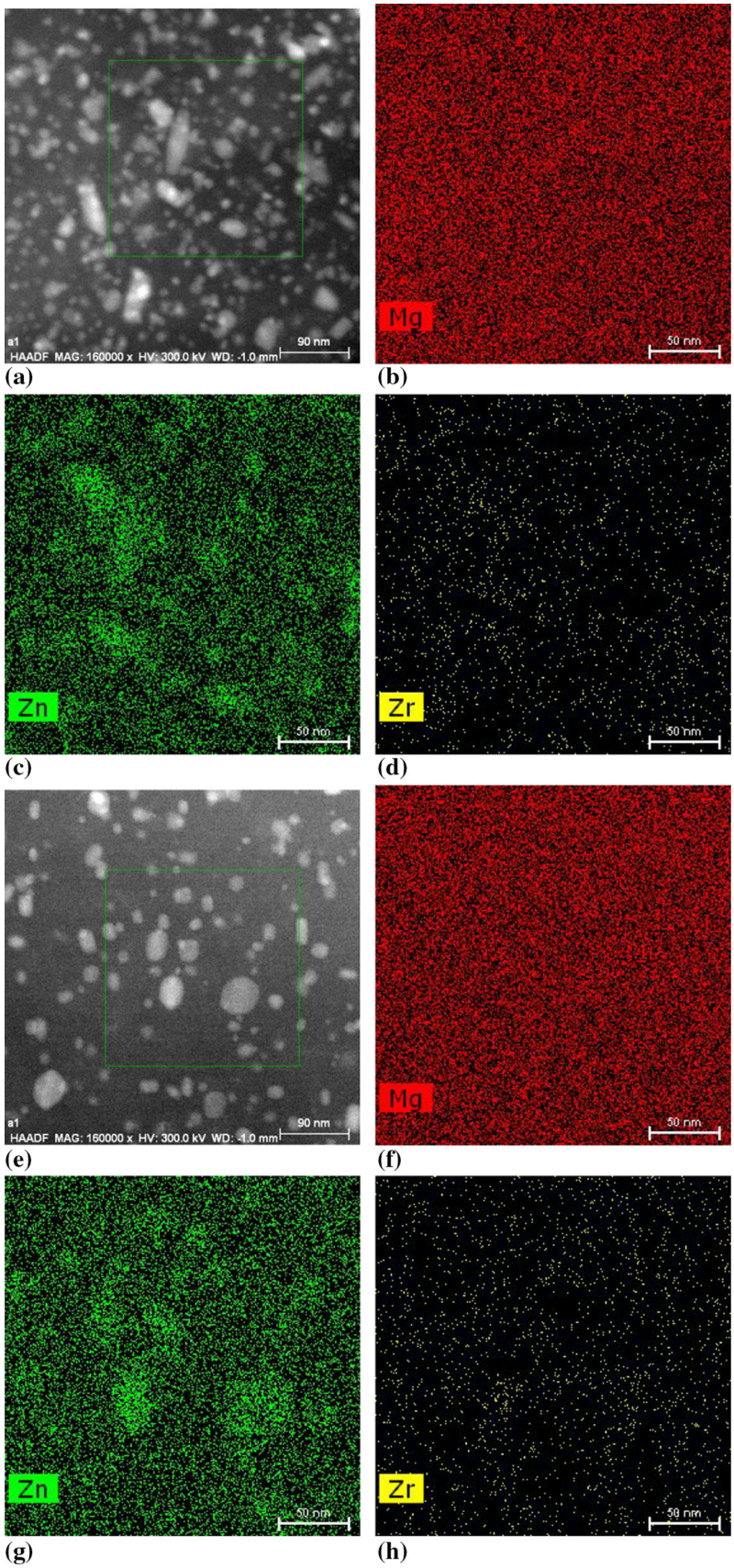


**Fig. 5** STEM images and elemental mappings of the as-rolled ZK60 sheets prepared by HSRR (a-d) and CR (e-h)

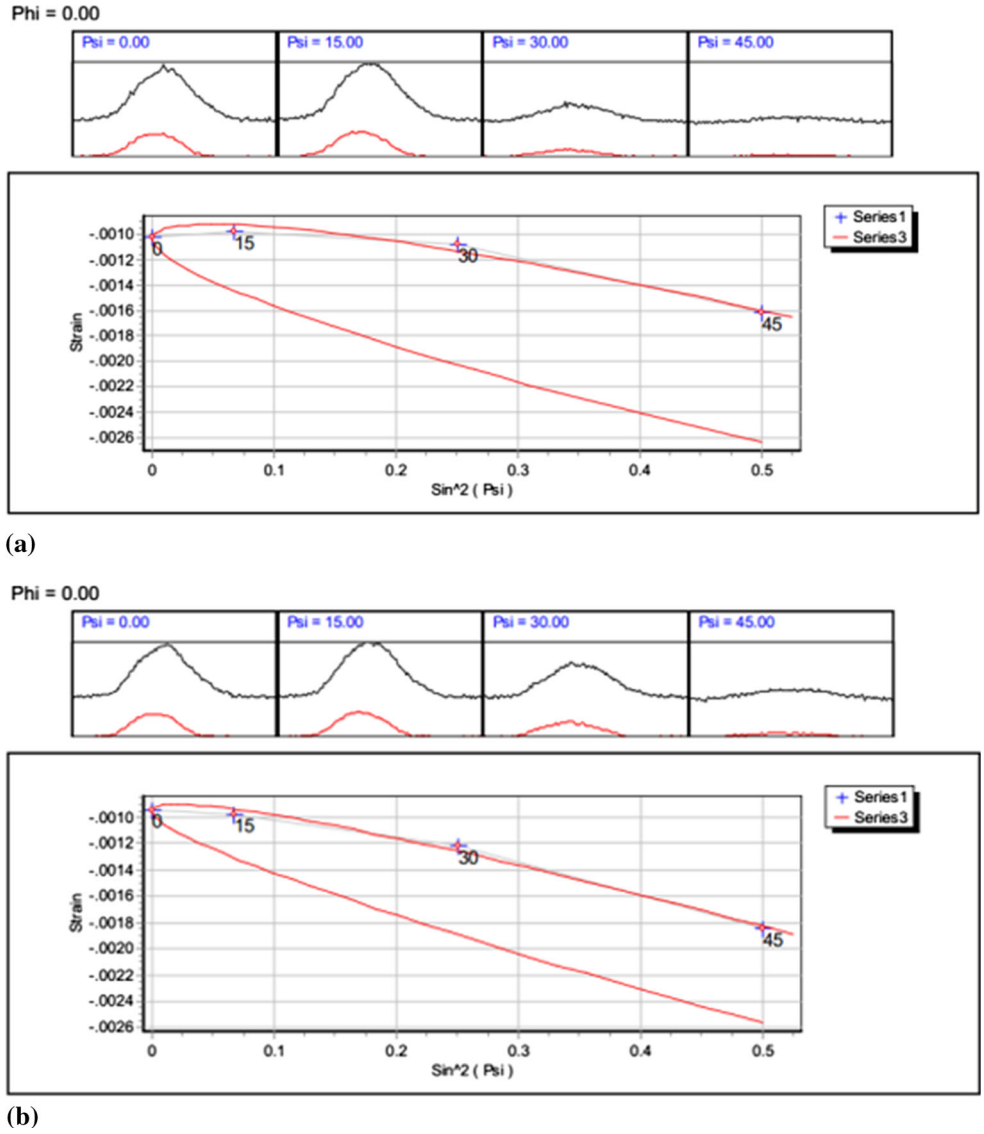


**Fig. 6** Residual stress distribution characteristics of the as-rolled ZK60 sheets

**Table 2 Residual stress data of the as-rolled ZK60 sheets**

| Rolling mode | European standard | | Chinese standard |
|---|---|---|---|
| | Residual normal stress, MPa | Residual shear stress, MPa | Residual stress, MPa |
| HSRR | −77.7 ± 16.4 | 18.6 ± 8.2 | −44.6 ± 13.2 |
| CR | −89.2 ± 11.8 | 13.2 ± 5.9 | −65.7 ± 9.4 |

average corrosion rate after 90 days immersion is 0.17 mg $cm^{-2}$ $d^{-1}$, about 19% lower than the CR sheet. Obviously, high strain rate rolling can reduce the corrosion rate of magnesium alloys in Hank's solution with the corresponding alloy prepared by CR as the control. As for the Mg-4Zn-0.3Ca alloy prepared by HSRR, its average corrosion rate after 90 days immersion is only 0.14 mg $cm^{-2}$ $d^{-1}$, much lower than the Mg-4Zn and ZK60 alloys in the HSRR state, indicating it is the most corrosion resistant except for pure Mg (99.99%).

**3.2.2 Electrochemical Behavior.** The typical electrochemical polarization curves of the as-rolled magnesium alloys prepared by HSRR and CR in Hank's solution at 37 °C are shown in Fig. 9. Electrochemical measurement results of the as-rolled magnesium alloys prepared by HSRR and CR in Hank's solution at 37 °C are listed in Table 3. All the curves are a bit symmetrical around the corrosion potential. As compared with the corresponding alloy prepared by CR, the curve of the as-rolled alloy prepared by HSRR reveals an obvious shift to the higher corrosion potential value. The corrosion potential of

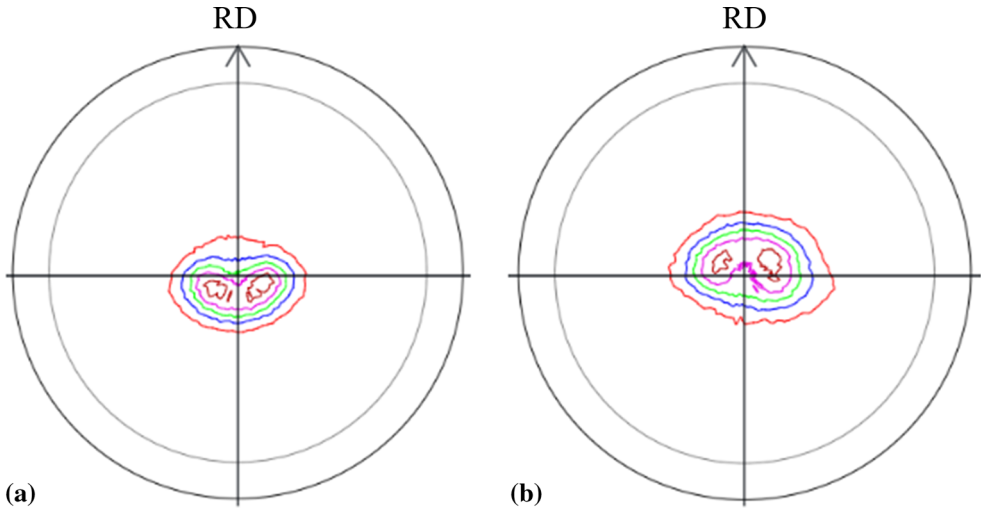


**Fig. 7** The (0001) pole figures of the as-rolled ZK60 sheets

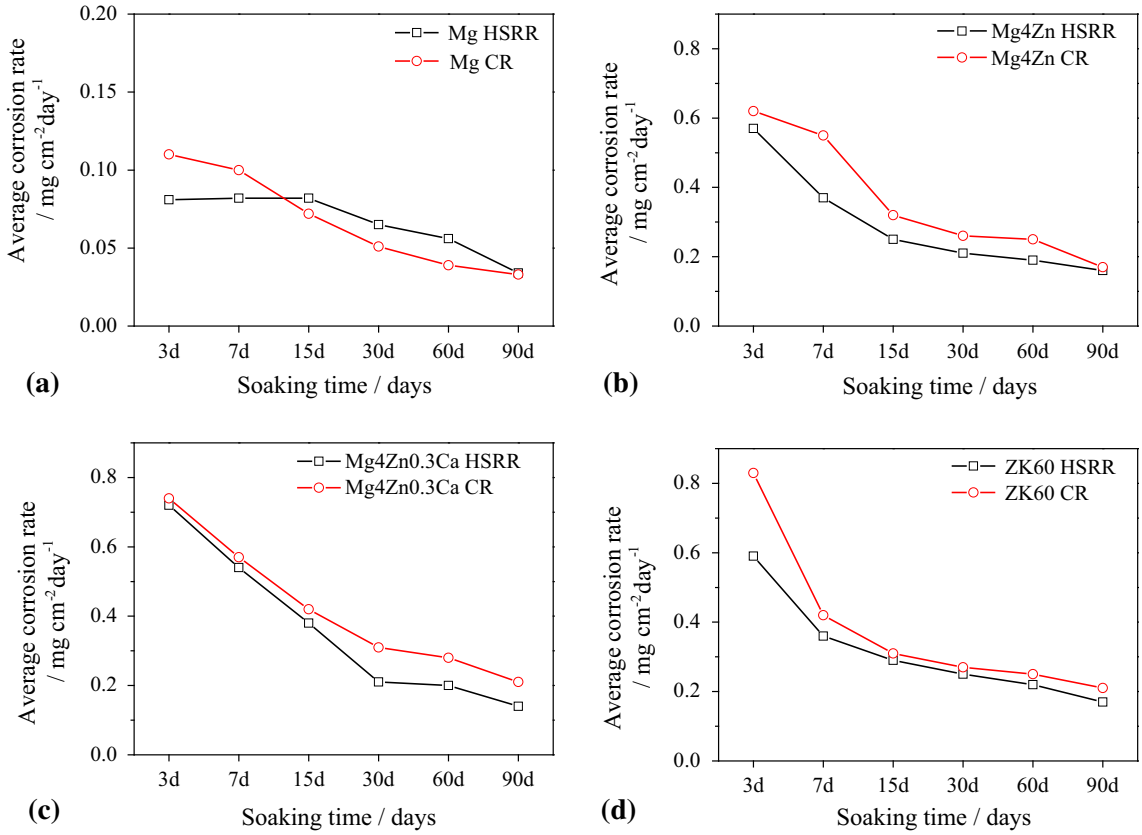


**Fig. 8** Average corrosion rate vs. soaking time curves of the as-rolled magnesium alloys prepared by HSRR and CR in Hank's solution at 37 °C

the HSRR pure Mg is −1.57 V, while that of the CR sheet is −1.59 V. The corrosion potential of the HSRR ZK60 alloy is −1.48 V, while that of the CR sheet is −1.50 V. Moreover, the corrosion current density value of HSRR is higher than the corresponding CR sample for every potential value on anodic curves, but it is just the reverse on cathodic curves.

However, the $\triangle E/\triangle \log I$ values in the cathodic branches are bigger than those in the anodic branches, indicating that the cathodic process plays a more important role in the alloy corrosion. The corrosion current density of the HSRR pure Mg is 1.0 μA/cm$^2$, while that of the CR sheet is 1.2 μA/cm$^2$. The corrosion current density of the HSRR Mg-4Zn alloy is 25.0 μA/cm$^2$, while that of the CR sheet is 29.0 μA/cm$^2$. The corrosion current density of the HSRR Mg-4Zn-0.3Ca alloy is 35.4 μA/cm$^2$, about 36% lower than the CR sheet. The corrosion current density of the HSRR ZK60 alloy is 30.9 μA/cm$^2$, about 45% lower than the CR sheet. The HSRR alloy has the higher corrosion potential and the lower corrosion current

density than the corresponding CR sheet, indicating that high strain rate rolling is more effective in bio-corrosion resistance improvement than conventional rolling. The electrochemical measurement is in good consistency with the weight loss measurement.

## 4. Discussion

On the basis of constant immersion testing (Fig. 8) and electrochemical measurement (Fig. 9), high strain rate rolling is more effective in enhancing bio-corrosion resistance of magnesium alloys in Hank's solution than conventional rolling. This phenomenon is related to the microstructural differences between the HSRR sheet and the CR sheet.

### 4.1 Effect of Grain Size and Twinning on Bio-Corrosion Resistance

As shown in Fig. 1, the HSRR sheet exhibits the higher DRX extent, the finer grain size and fewer twins than the corresponding CR sheet. It is reported that grain refinement is beneficial to corrosion improvement in the corrosion of the untwinned microstructure (Ref 18). The grain boundary acts as a physical corrosion barrier, and thus, the corrosion rate in small-grained microstructure slows down compared with coarse-grained microstructure. Clearly, grain refinement induced by high strain rate rolling is beneficial to corrosion resistance improvement for the HSRR alloy. According to Aung A A et al. (Ref 18), the existence of twins can further accelerate the corrosion and the corrosion rate significantly increases with the average grain size increasing from 65 to 250 μm in the corrosion of the untwinned microstructure. According to Hamu G B et al. (Ref 9), the effect of grain size is less pronounced in the corrosion of the twinned microstructure and a higher density of dislocation and twins probably lead to high anodic dissolution. In comparison with the CR alloy, the HSRR alloy has fewer twins and lower dislocation density than the corresponding CR alloy and thus it is more corrosion resistant in Hank's solution. However, it is also reported that the corrosion resistance of AZ31B alloy tends to increase as grain size is reduced, probably due to the enhanced passivity of surface oxide film, while the effect of grain size is not as significant as that of chemical compositions (Ref 19). This is not in agreement with the present study. As for pure Mg, no second phases are involved. The HSRR pure Mg sheet exhibits the lower corrosion rate within 10 days, the higher corrosion potential and the lower current density than the CR sheet. Therefore, the HSRR sheet featured with finer grain size and fewer twins exhibits better bio-corrosion resistance than the corresponding CR alloy.

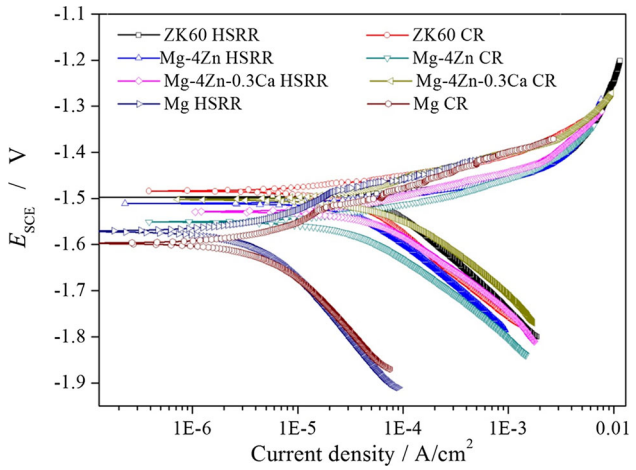


**Fig. 9** Typical electrochemical polarization curves of the as-rolled magnesium alloys prepared by HSRR and CR in Hank's solution at 37 °C

As shown in Fig. 9, the corrosion current density values of HSRR are higher than the corresponding CR sample for every potential value on anodic curves, while it is just the reverse on cathodic curves, indicating that higher anodic dissolution is associated with HSRR than CR. However, the HSRR alloy has fewer twins and lower dislocation density than the corresponding CR alloy, which means the lower anodic dissolution. The detailed reason for the contradictory remains unclear.

### 4.2 Effect of Second Phases on Bio-Corrosion Resistance

The as-rolled ZK60 alloys are mainly composed of three phases, i.e., the α-Mg matrix, the residual $Mg_7Zn_3$ phase and the $\beta_1$ phase precipitating both in the grain interiors and at grain boundaries. The Mg-Zn phases play the different role in the degradation process. On the one hand, the intermetallics such as $Mg_7Zn_3$, $Mg_{17}Al_{12}$, $Mg_2Sn$ always act as the cathode and thus many primary cells between α-Mg and $Mg_7Zn_3$ are existent in the as-rolled alloys during the immersion. The α-Mg matrix surrounding the second phases acts as micro-anode to be corroded preferentially. On the other hand, it can be supposed that electrolytes can penetrate into the inner of the alloy due to the increase in the α-Mg and $Mg_7Zn_3$ couples with a higher potential and thus the corrosion rate is increased. Therefore, the existence of the $Mg_7Zn_3$ phase is detrimental to bio-corrosion resistance. According to Song Y W et al. (Ref 20), the corrosion resistance of the Mg-xZn alloys in 3.5%NaCl solution reduces with increasing Zn concentration, which is mainly attributed to the cathodic effect of the $Mg_xZn_y$ second phases on the corrosion resistance.

As shown in Fig. 3 and marked by the black circles, the remained $Mg_7Zn_3$ particles in the HSRR ZK60 sheet are in granular and are distributed along the primary grain boundaries, while those in the CR sheet are broken and are elongated along the rolling direction. In compared with the CR sheet, the

**Table 3 Electrochemical data of the as-rolled sheets**

| | Pure Mg | | Mg-4Zn | | Mg-4Zn-0.3Ca | | ZK60 | |
|---|---|---|---|---|---|---|---|---|
| **Alloys** | **HSRR** | **CR** | **HSRR** | **CR** | **HSRR** | **CR** | **HSRR** | **CR** |
| $E_{corr}$, V | −1.57 | −1.59 | −1.51 | −1.55 | −1.51 | −1.53 | −1.48 | −1.50 |
| $i_{corr}$, μA/cm$^2$ | 1.0 | 1.2 | 25.0 | 29.0 | 35.4 | 54.9 | 30.9 | 56.2 |

$Mg_7Zn_3$ particles in the HSRR ZK60 alloy are relatively coarse and are in micron scale. Thus, more primary cells between α-Mg and $Mg_7Zn_3$ are involved in the CR ZK60 alloy due to the severe breakup of the $Mg_7Zn_3$ phase. Moreover, the large area of the cathode and the reduced ratio of cathode to anode are associated with the refinement of the micron-size $Mg_7Zn_3$ phase and thus the accelerated corrosion of the matrix is involved. The cross-sectional morphologies of ZK60 soaked in Hank's solution for 12 h are shown in Fig. 10. The corrosion pits of the HSRR alloy are relatively low, about 6 μm in depth; those of the CR alloy are relatively deep, about 23 μm in depth. Since more primary cells are formed in the CR alloy, the accelerated corrosion of the matrix is involved and more corrosion pores are formed. These corrosion pores are connected into the larger corrosion pits (Ref 16). Therefore, bio-corrosion resistance improvement of magnesium alloys by HSSR is likely related to the relatively big size of the residual second phase.

As seen from Fig. 4(f) and (h), the nanometer precipitates in the grain interiors of the HSRR ZK60 sheet are much finer and denser than those in the CR sheet. These nanometer precipitates are inferred to be the $\beta_1$ phase. According to Gao J H et al., high-pressure torsion can improve bio-corrosion resistance of the Mg-2Zn-0.24Ca alloy and this effect is associated with the delay of corrosion process by the homogeneous nanoscale precipitates with some certain orientation relationships in the grain interiors and the homogeneous corrosion derived from the uniform distribution of nanometer precipitates (Ref 8). According to Mostaed E et al. (Ref 21), an improved corrosion resistance of UFG ZK60 alloy compared to the extruded one stems from a shift of corrosion regime from localized pitting in the as-received sample to a more uniform corrosion mode with reduced localized attack in ECAP-processed alloy and ECAP-induced second-phase redistribution markedly depresses localized corrosion. The $\beta_1$ phase has two certain orientation relationships with the Mg matrix. It is speculated that the nanometer $\beta_1$ precipitates are beneficial to delay the corrosion process of ZK60 alloy. The HSRR ZK60 alloy exhibits better bio-corrosion resistance than the CR alloy since the finer and denser nanometer $\beta_1$ precipitates are involved. Effects of the nanoscale precipitates on corrosion resistance of the Mg-Zn system are being undertaken.

### 4.3 Effect of Residual Stress on Bio-Corrosion Resistance

Residual stresses are produced when one region of a part experiences permanent plastic deformation, while other regions of the same part either remain elastic or are plastically deformed to a different degree (Ref 22). Generally, tensile stresses are undesired as they may cause a decrease in fatigue life, performance in corrosive environments and delaminating. However, compressive stresses are always beneficial to prevent stress corrosion cracking. Up to now, almost no study on effects of the compressive stress level on corrosion resistance of magnesium alloys has been reported. As stated above, the as-rolled ZK60 sheets are featured with the residual normal compressive stress state and the HSRR ZK60 sheet exhibits the lower residual normal stress than the CR sheet. The latter indicates that the higher density of dislocation and the higher storage energy are involved in the CR sheet, which would induce the higher chemical activity. According to Pu Z et al. (Ref 23), the remarkably improved corrosion resistance of AZ31 in NaCl solution after severe plasticity burnishing is attributed mainly to dramatically reduced grain size and strongly basal-textured grain orientation and residual stresses have less influence than texture and grain size. Therefore, residual stress should not be considered as the crucial factor for the difference in bio-corrosion resistance of the HSRR and the CR alloys.

### 4.4 Effect of Texture on Bio-Corrosion Resistance

The texture characteristics have obvious influence on corrosion resistance of magnesium alloys (Ref 21, 23, 24). It is reported that the stronger basal texture is beneficial to the remarkably improved corrosion resistance of AZ31 in NaCl solution (Ref 23). It is also reported that the AZ31 sample with c-axis of most grains normal to the exposed surface exhibits much higher corrosion resistance in simulated body fluid than the sample consisting mainly of (10-10) and (11-20) oriented grains at the early immersion time (Ref 24). According to G. L. Song (Ref 25), the different surfaces of hot-rolled AZ31 sheet dominated by different crystal planes have very different corrosion performance and the (0001) basal plane-dominated rolling surface is more corrosion resistant than the cross-section surface that is mainly composed of (10-10) and (11-20) prismatic planes. As shown in Fig. 7, the ZK60 sheet prepared by HSRR has a slightly stronger basal texture than the sheet prepared by CR. As shown in Fig. 8 and 9, the HSRR sheet exhibits better bio-corrosion resistance than the corresponding CR alloy. In this sense, the stronger basal texture is probably one factor for the improved bio-corrosion resistance of the HSRR ZK60 alloy.

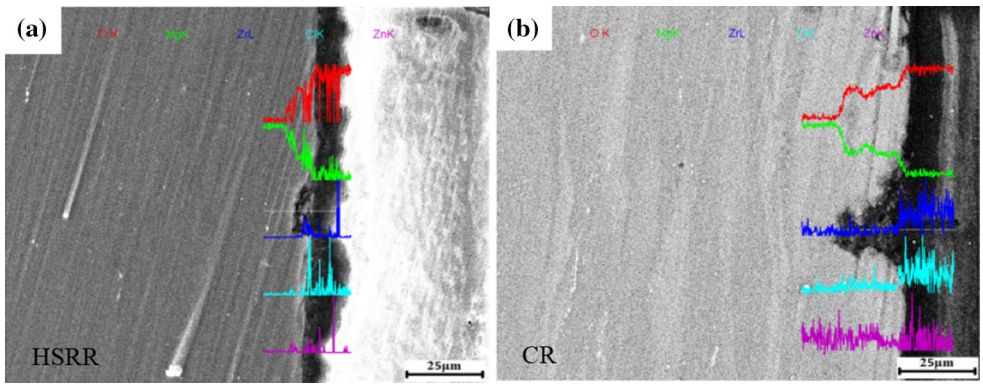


**Fig. 10** Cross-sectional morphologies of ZK60 soaked in Hank's solution for 12 h

In summary, bio-corrosion resistance improvement of ZK60 alloy by HSRR can be ascribe to the reduced grain size, relatively adequate DRX, lack of twinning, the relatively big size of the residual second phase, the finer and denser nanometer $\beta_1$ precipitates and the slightly stronger basal texture. The profound microstructural effects on the corrosion resistance in Hank's solution open a new window to control the corrosion property of Mg alloys for biomedical applications. It is desirable to find the usage in the field of bone fixation. The in vivo experiments and the detailed corrosion mechanisms are undertaken.

## 5. Conclusions

Microstructure and bio-corrosion resistance in Hank's solution of four magnesium alloy sheets (pure Mg, ZK60, Mg-4Zn and Mg-4Zn-0.3Ca) prepared by high strain rate rolling and conventional rolling are comparatively investigated. The microstructural effects on the corrosion resistance of magnesium alloys in Hank's solution are drawn as the following.

1. The HSRR alloy exhibits better bio-corrosion resistance than the corresponding CR alloy. The average corrosion rate of the HSRR ZK60 sheet after 90-day immersion in Hank's solution is 0.17 mg $cm^{-2}$ $d^{-1}$, about 19% lower than the CR sheet. Its corrosion current density is 30.9 $\mu A/cm^2$, about 45% lower than the CR sheet.
2. The HSRR ZK60 alloy is featured with finer grains, the higher DRX extent, the lower twin fraction, the relatively coarse second-phase particles, the lower residual compressive stress, the finer and denser nanometer $\beta_1$ precipitates and the slightly stronger basal texture than the CR alloy.
3. Bio-corrosion resistance improvement of magnesium alloys by HSRR can be mainly ascribe to the reduced grain size, the relatively adequate DRX, lack of twinning, the relatively big size of the residual second phase, the finer and denser nanometer precipitates and the slightly stronger (0001) texture.


### Acknowledgments

The authors are grateful to the support of the Natural Science Foundation Project of China (51571089), the Young Teacher Growth Fund of Hunan University (531107021095) and the National SIT Project.


### References


1. F. Witte, The History of Biodegradable Magnesium Implants: A Review, *Acta Biomater.*, 2010, **6**, p 1680–1692
2. F. Witte, V. Kaese, H. Haferkamp, E. Switzer, A. Meyer-Lindenberg, and C.J. Wirth, In Vivo Corrosion of Four Magnesium Alloys and the Associated Bone Response, *Biomaterials*, 2005, **26**, p 3557–3563
3. H. Wang, Y. Estrin, and Z. Zúberová, Bio-Corrosion of a Magnesium Alloy with Different Processing Histories, *Mater. Lett.*, 2008, **62**, p 2476–2479
4. S.E. Harandi, M.H. Idris, and H. Jafari, Effect of Forging Process on Microstructure, Mechanical and Corrosion Properties of Biodegradable, *Mg-1Ca alloy*, 2011, **32**, p 2596–2603
5. H.Y. Choi and W.J. Kim, Effect of Thermal Treatment on the Bio-Corrosion and Mechanical Properties of Ultrafine-Grained ZK60 Magnesium Alloy, *J. Mech. Behav. Biomed. Mater.*, 2015, **51**, p 291–301
6. P. Minárik, R. Kral, and M. Janeček, Effect of ECAP Processing on Corrosion Resistance of AE21 and AE42 Magnesium Alloys, *Appl. Surf. Sci.*, 2013, **281**, p 44–48
7. D.X. Liu, C.G. Guo, L.Q. Cai, V.R. Sherman, X.Q. Qin, Y.T. Ding, and M.A. Meyers, Mechanical Properties and Corrosion Resistance of Hot Extruded Mg-2.5Zn-1Ca Alloy, *Mater. Sci. Eng., C*, 2013, **33**, p 2345–2352
8. J.H. Gao, S.K. Guan, Z.W. Ren et al., Homogeneous Corrosion of High Pressure Torsion Treated Mg-Zn-Ca Alloy in Simulated Body Fluid, *Mater. Lett.*, 2011, **65**, p 691–693
9. G.B. Hamu, D. Eliezer, and L. Wagner, The Relation Between Severe Plastic Deformation Microstructure and Corrosion Behavior of AZ31 Magnesium Alloy, *J. Alloy. Compd.*, 2009, **468**, p 222–229
10. H. Zhang, W.L. Cheng, J.F. Fan, B.S. Xu, and H.B. Dong, Improved Mechanical Properties of AZ31 Magnesium Alloy Sheets by Repeated Cold Rolling and Annealing Using a Small Pass Reduction, *Mater. Sci. Eng., A*, 2015, **637**, p 243–250
11. H. Zhang, G.S. Huang, J.F. Fan, H.J. Roven, F.S. Pan, and B.S. Xu, Deep Drawability and Deformation Behavior of AZ31 Magnesium Alloy Sheets at 473 K, *Mater. Sci. Eng., A*, 2014, **608**, p 234–241
12. S.Q. Zhu, H.G. Yan, J.H. Chen, Y.Z. Wu, J.Z. Liu, and J. Tian, Effect of Twinning and Dynamic Recrystallization on the High Strain Rate Rolling Process, *Scripta Mater.*, 2010, **63**(10), p 985–988
13. S.Q. Zhu, H.G. Yan, X.Z. Liao, S.J. Moody, G. Sha, Y.Z. Wu, and S.P. Ringer, Mechanisms for Enhanced Plasticity in Magnesium Alloys, *Scripta Mater.*, 2015, **82**, p 344–355
14. Z.Y. Zou, J.H. Chen, H.G. Yan, B. Su, and X.L. Gong, Microstructure, Bio-Corrosion Behavior and Corrosion Residual Strength of High Strain Rate Rolled Mg-4Zn Alloy Sheet, *J. Mater. Eng. Perform.*, 2016, **25**, p 1974–1985
15. J.H. Chen, Z.Y. Zou, H.G. Yan, B. Su, R.H. Xie, Y.J. Yang, X.L. Gong, and J.L. Huang, Effects of High Strain-Rate Rolling on Microstructure and Properties of the Mg-4Zn Alloy. *Rare Metal Mater. Eng.*, 2017, **46**, p 2220–2226 (in Chinese)
16. J.H. Chen, G.Q. Chen, H.G. Yan, B. Su, and X.L. Gong, Effects of Rolling Mode On Bio-Corrosion Behavior of Magnesium Alloys, *J. Hunan Univ. (Nat. Sci.)*, 2016, **12**, p 24–30 (in Chinese)
17. S. Q. Zhu. An Exploratory Study on the Principle of the Fabrication of Ultrafine Grained Magnesium Sheets Using Medium-High Strain Rate Rolling Technique and the Related Fundamental Research. Doctoral Thesis, Hunan University
18. N.N. Aung and W. Zhou, Effect of Grain Size and Twins on Corrosion Behaviour of AZ31B Magnesium Alloy, *Corros. Sci.*, 2010, **52**, p 589–594
19. J.S. Liao, M. Hotta, and N. Yamamoto, Corrosion Behavior of Fine-Grained AZ31B Magnesium Alloy, *Corros. Sci.*, 2012, **61**, p 208–214
20. Y.W. Song, E.H. Han, D.Y. Shan, C.D. Yim, and B.S. You, The Effect of Zn Concentration on the Corrosion Behavior of Mg-xZn Alloys, *Corros. Sci.*, 2012, **65**, p 322–330
21. E. Mostaed, M. Hashempour, A. Fabrizi, D. Dellasega, M. Bestetti, F. Bonollo, and M. Vedani, Microstructure, Texture Evolution, Mechanical Properties and Corrosion Behavior of ECAP Processed ZK60 Magnesium Alloy for Biodegradable Applications, *J. Mech. Behav. Biomed.*, 2014, **37**, p 307–322
22. B.L. Averbach and L. Binghe, Fatigue Crack Propagation Through Residual Stress Field, *Ad. Fracture Res.*, 1984, **3**, p 1631–1640
23. Z. Pu, G.L. Song, S. Yang, J.C. Outeiro, O.W. Dillon, Jr., D.A. Puleo, and I.S. Jawahir, Grain Refined and Basal Textured Surface Produced by Burnishing for Improved Corrosion Performance of AZ31B Mg Alloy, *Corros. Sci.*, 2012, **57**, p 192–201
24. R.L. Xin, Y.M. Luo, A.L. Zuo, J.C. Gao, and Q. Liu, Texture Effect on Corrosion Behavior of AZ31 Mg Alloy in Simulated Physiological Environment, *Mater. Lett.*, 2012, **72**, p 1–4
25. G.L. Song, The Effect of Texture Effect on the Corrosion Behavior of AZ31 Mg Alloy, *JOM*, 2012, **64**, p 671–679